PIER M

(Received 24 January 2024, Accepted 25 March 2024, Scheduled 2 April 2024)

An Antipodal Vivaldi Antenna with a Lower Cutoff Frequency Based on Spoof Surface Plasmon Polaritons and Corrugated Edges

Baoping Ren, Chenguang Zhao, Xuehui Guan, and Shaopeng Wan*

School of Information Engineering, East China Jiaotong University, Nanchang 330013, China

ABSTRACT: In this paper, an antipodal Vivaldi antenna (AVA) with a lower cutoff frequency is proposed based on spoof surface plasmon polaritons (SSPPs) and corrugated edges. Firstly, the gradient slots are etched on the outer edges of the two radiation arms of the conventional antipodal Vivaldi antenna. As a result, the low cutoff frequency is decreased slightly due to the increased surface current path of the antenna. More importantly, the SSPPs structure with identical units is etched on the inner side of two radiation arms, leading to a significant reduction in the low cutoff frequency due to the larger propagation constant of the SSPPs structure compared to the radiation arms of the conventional antipodal Vivaldi antenna. Additionally, the structure of the SSPPs on the stripline ensures effective momentum and mode matching between the quasi-TEM mode and SSPPs mode. Furthermore, to improve the gain at the high-frequency band, the structure of the SSPPs introduced on the inner side of the two radiation arms is further optimized by varying the depths of the grooves. Experimental results demonstrate that the designed antipodal Vivaldi antenna exhibits excellent radiation performance, with a low cutoff frequency of 2.8 GHz and a maximum gain of 9.3 dBi.

1. INTRODUCTION

Antipodal Vivaldi antenna (AVA) is an ultra-wideband antenna that demonstrates high gain and stable radiation characteristics. It has been widely used in various scenarios, including 5G communication [1], radar [2], imaging applications [3], and industrial sensors [4]. However, due to limitations in the dimensions of the radiation section in most realistic scenarios, the antenna has a low cutoff frequency. This limitation restricts the applications of antipodal Vivaldi antennas, prompting the proposal of numerous methods [5–17] aimed at overcoming it. These methods include using a substrate with a high dielectric constant [5], high chip resistor loading technology [6], a cavity-backed structure [7], a stepped connection structure [8], metamaterials loading technology [9], radiating arms shaping [10, 11], and corrugated edges [12–14]. Corrugated edges are the most widely used method to reduce the low cutoff frequency; however, their effectiveness is limited and requires combined use with other techniques [15–17].

Spoof surface plasmon polaritons (SSPPs), which are produced by metallic grooves on a substrate, demonstrate characteristics such as a large propagation constant, strong field confinement, and deep-subwavelength properties, akin to surface plasmon polaritons (SPPs) in the optical frequency range [18]. These electromagnetic properties can be manipulated by adjusting the parameters of the grooves [19]. The distinctive characteristics of SSPPs have attracted considerable attention in electromagnetic manipulation and have been the focus of research for decades [20–25]. Among these explorations, the research on miniaturizing antennas using SSPPs stands out [20–22]. In [20], a method for miniaturizing dipole antennas has been developed based on spoof surface plasmon polaritons, which possess a large propagation constant, allowing for a dramatic reduction in the guided wavelength. In [21], based on the deep-subwavelength property of the spoof surface plasmon polaritons, a method for miniaturizing the monopole antenna is proposed.

A novel method to effectively extend the low cutoff frequency of the antipodal Vivaldi antenna based on SSPPs and corrugated edges is proposed in this paper. The structure was designed with periodic grooves etched on the stripline, the inner and outer sides of the radiating arms. The depth of the grooves etched on the end of the stripline is gradually reduced to ensure good mode and momentum matching between the quasi-TEM mode and SSPPs mode. Moreover, the guided wavelength is shortened by inner-side etched grooves on the radiating arms, while outer-side etched grooves extend the surface current path. As a result, the low cutoff frequency of the antenna is decreased, achieving its purpose of miniaturization. In comparison to the original antipodal Vivaldi antenna, the proposed corrugated edges loading technology and SSPPs-based antipodal Vivaldi antenna offer the advantages of a lower cutoff frequency and higher gain in the low-frequency band.

2. ANTENNA DESIGN AND ANALYSIS

The original AVA (OAVA) is a traditional antipodal Vivaldi antenna implemented on a Rogers 4003C substrate with a relative permittivity of 3.55 and a thickness of 0.508 mm, as shown in the configuration in Fig. 1(a). It is a double-layer design, including a microstrip-fed section, a stripline transmission sec-

* Corresponding author: Shaopeng Wan (906804909@qq.com).

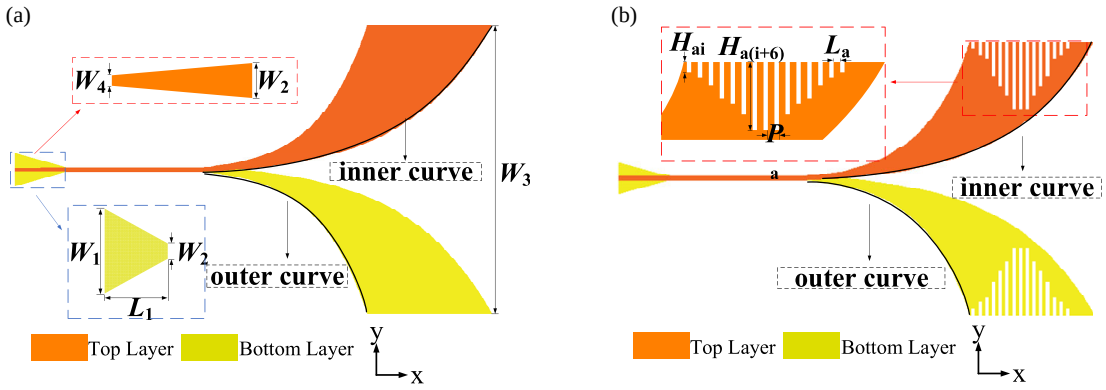

FIGURE 1. (a) Configuration of the OAVA. (b) Configuration of Antenna I.

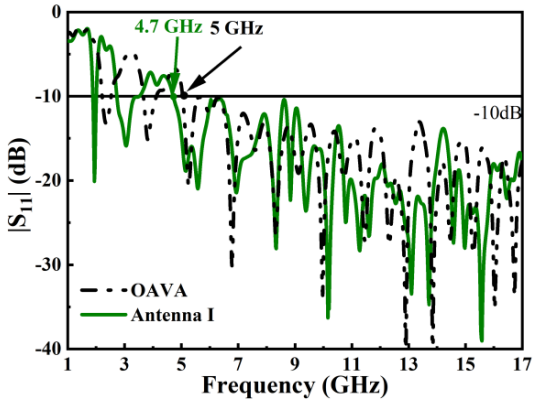

FIGURE 2. Simulated $|S_{11}|$ of the OAVA and Antenna I.

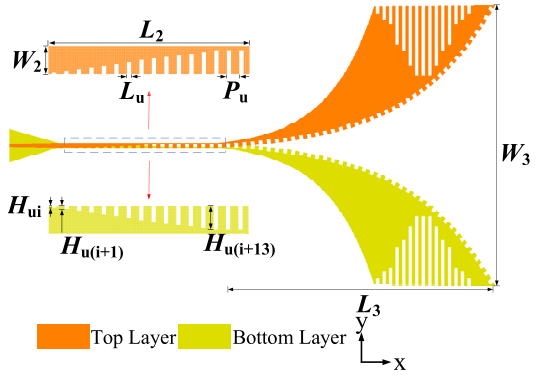

FIGURE 3. Configuration of Antenna II.

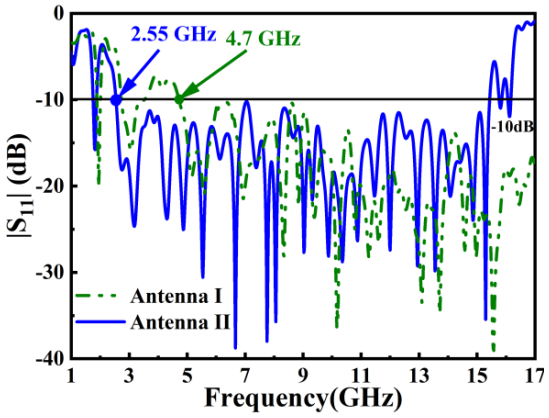

FIGURE 4. Simulated $|S_{11}|$ of Antenna I and Antenna II.

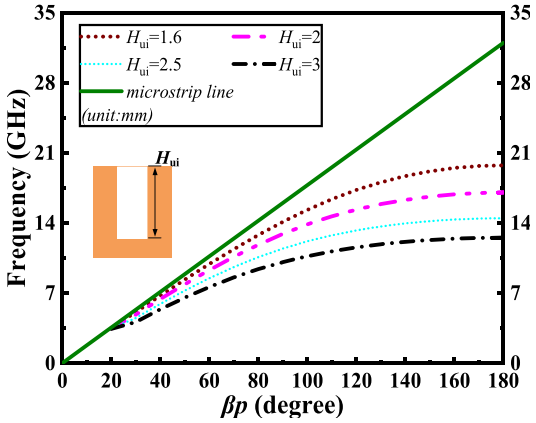

FIGURE 5. Dispersion curve.

tion, and an antipodal Vivaldi radiation section. The equation of the antipodal Vivaldi curves is described in [26] as

$$y = \pm a_1 \exp(\alpha x) + a \tag{1}$$

Based on (1), the inner curve is designed by $\alpha = 0.07$, $a = 0$ mm, and $a_1 = 1.5$ mm, and the outer curve is described by $\alpha = 0.04$, $a = -1.5$ mm, and $a_1 = 1.5$ mm.

Etching slots on the outer side of the radiating arms is a method that can reduce the low cutoff frequency. As shown in Fig. 1(b), Antenna I is obtained by etching slots on the outer side of radiating arms in OAVA. Fig. 2 illustrates the $|S_{11}|$ of the OAVA and Antenna I, indicating a slight decrease in the low cutoff frequency from 5 GHz to 4.7 GHz. To further decrease the low cutoff frequency of Antenna I, we propose an improved antipodal Vivaldi antenna, denoted as Antenna II. This is achieved by etching grooves with a height gradient on the stripline and grooves with the same height on the inner side of the radiation arms, as shown in Fig. 3.

Figure 4 displays the simulated $|S_{11}|$ of Antenna I and Antenna II. The low cutoff frequency of Antenna II is observed

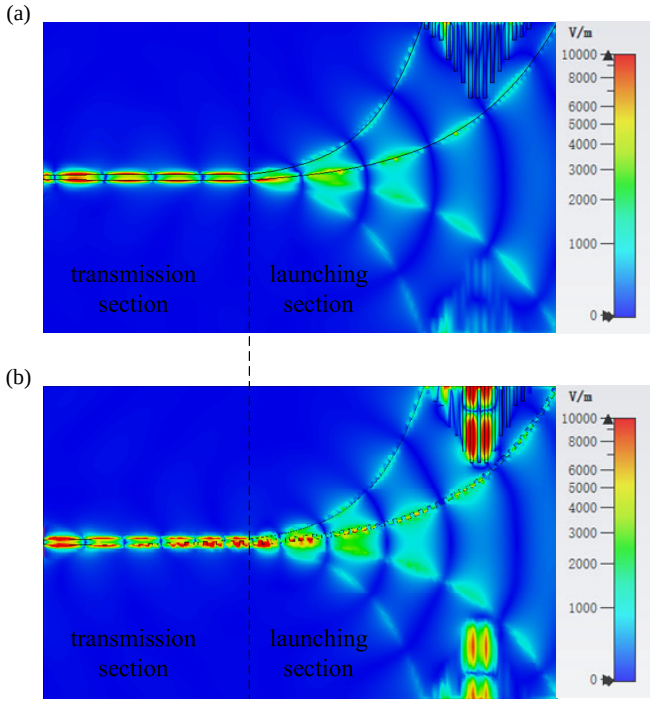

FIGURE 6. The E-fields distribution of (a) Antenna I and (b) Antenna II at 8 GHz.

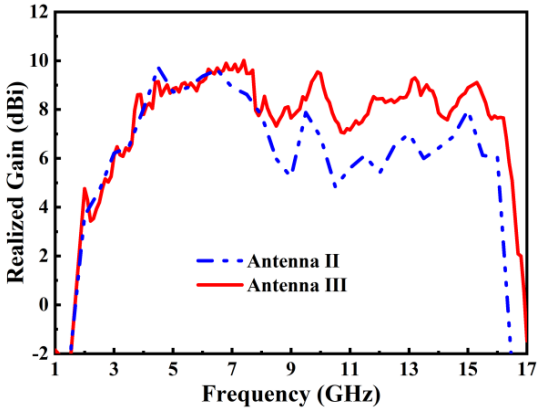

FIGURE 7. Gain of Antenna II and Antenna III.

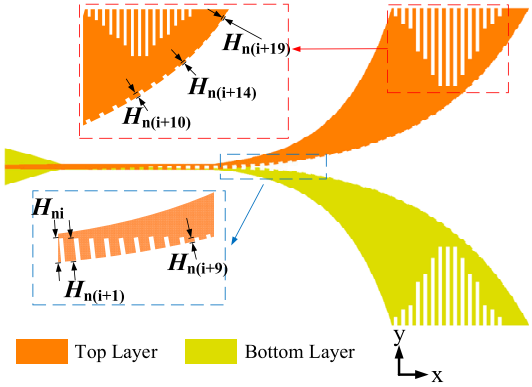

FIGURE 8. Configuration of Antenna III.

to be lower than that of Antenna I, with the frequency decreasing from 4.7 GHz to 2.55 GHz. As mentioned in [27], antenna miniaturization can be achieved by decreasing the low cutoff frequency. Therefore, Antenna II is miniaturized compared to the OAVA.

As shown in Fig. 5, it is evident that the dispersion curve of the SSPPs unit deviates increasingly away from that of the microstrip line as H_{ui} increases. This indicates that the SSPPs structure can achieve a larger propagation constant than the microstrip line, leading to a reduction in the wavelength. This is illustrated by the electric field distribution in Fig. 6(a) and Fig. 6(b). In Fig. 1(a), W_3 is the width of the antenna and is the section where the slot is the widest. This radiates the longest wavelength electromagnetic wave corresponding to the low cutoff frequency [28]. As the wavelength shortens, the radiation region shifts towards a narrower slot. Consequently, the original cutoff frequency in Antenna II is replaced by a lower frequency, thereby reducing the low cutoff frequency.

Figure 7 shows the simulated results for antenna gain. It has been observed that a sudden change occurs at a specific frequency point effectively suppressing the splitting of the main lobe. However, the gain curve of Antenna II exhibits a significant drop in the high-frequency range.

Based on the dispersion curve, higher frequencies or taller SSPPs units result in a stronger field constriction. When Antenna II operates at high frequencies, the strong field constriction of SSPPs on the electromagnetic wave causes some of the energy to remain unreleased. This, in turn, affects the distribution of surface currents within the radiation arms. Consequently, this effect leads to adverse consequences such as main beam splitting, distortion of the radiation pattern, and increased levels of side lobes.

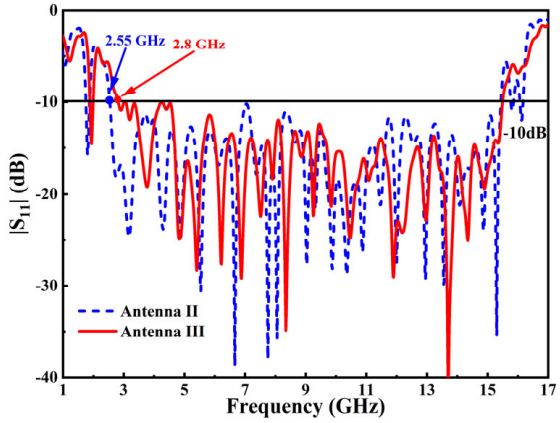

FIGURE 9. Simulated $|S_{11}|$ of the Antenna II and Antenna III.

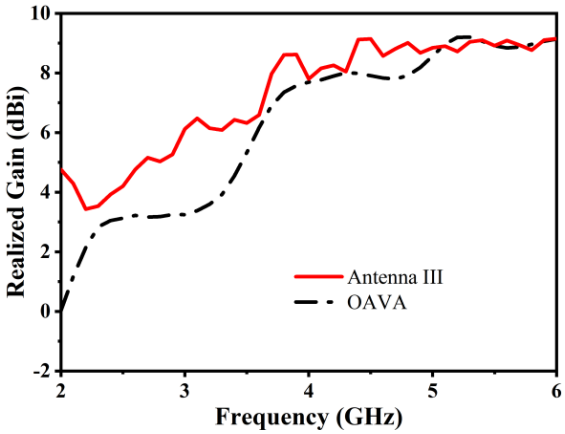

FIGURE 10. Gain of OAVA and Antenna III in low frequency band.

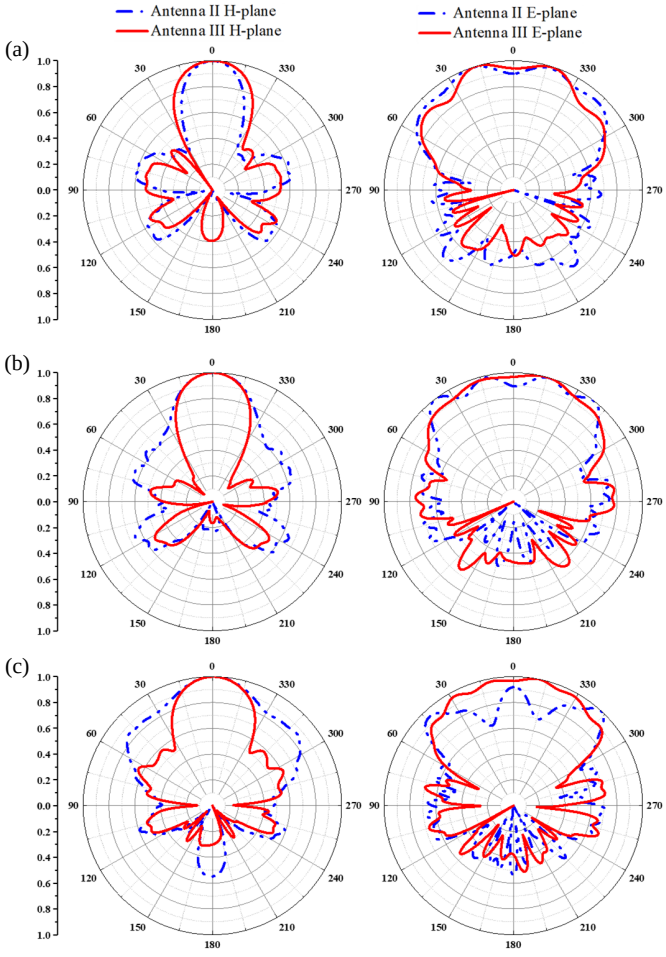

FIGURE 11. Normalized E-plane/H-plane radiation patterns of Antenna II and Antenna III at (a) 10.5 GHz, (b) 12 GHz, and (c) 15 GHz.

To address the aforementioned issue and improve the antenna's performance at high frequencies, a new antipodal Vivaldi antenna with height gradient grooves on the inner side of the radiation arms, referred to as Antenna III, is proposed, as shown in Fig. 8. This design aims to achieve a gradual release of electromagnetic energy. The height variation for the SSPPs unit follows the following rules: In the initial section of the radiating part, the height gradually decreases from 1.2 mm with a step size of 0.1 mm until it reaches 0.2 mm. In the terminal section of the radiating part, the height gradually decreases from 0.2 mm with a step size of 0.01 mm, ultimately reaching 0.1 mm.

Similarly, the simulated $|S_{11}|$ for proposed antenna is shown in Fig. 9. It is observed that the low cutoff frequency is a slightly increased due to the reduction in the height of the SSPPs units located on the inner side of the radiating arms.

The gain of OAVA and Antenna III in low frequency band is demonstrated in Fig. 10. Antenna III exhibits enhanced gain compared to the OAVA in the frequency band of 2.5–5 GHz, plateauing at approximately 5.1 GHz.

Figures 11(a)–(c) display the normalized E-plane and H-plane radiation patterns of Antenna II and Antenna III at different frequencies. The comparison reveals that at various frequencies, Antenna III can partly suppress main beam splitting and reduce the level of side lobes, but it does not totally eradicate main beam splitting, which is why the gain of Antenna III is a little bit low in the high frequency band.

TABLE 1. Geometric parameters of the proposed antenna. (Units: mm).

Parameters	Value	Parameters	Value
W_1	10	P_a	2
L_1	15	L_a	1
W_2	1.5	H_{a7}	21
L_2	40.96	H_{u1}	0.1
W_3	85.4	H_{u2}	0.13
L_3	85	H_{u3}	0.16
W_4	1.06	H_{u4}	0.2
L_u	1.2	ΔH_u	0.1
P_u	2.5	H_{u14}	1.2

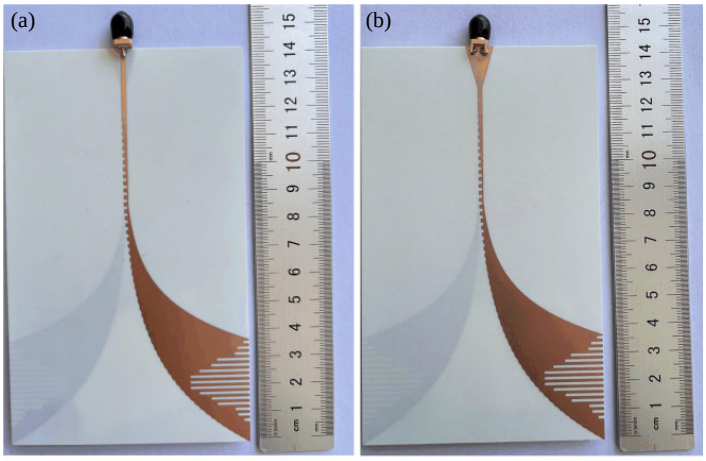

FIGURE 12. Photographs of the antenna: (a) Top layer, (b) bottom layer.

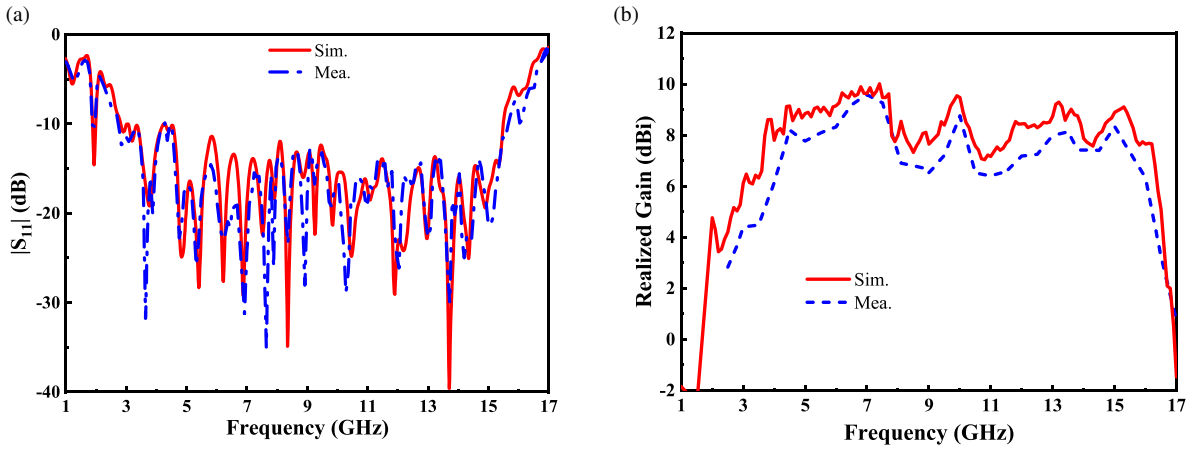

FIGURE 13. Simulated and measured results of Antenna III. (a) $|S_{11}|$. (b) Gain curve.

3. EXPERIMENTAL RESULT AND COMPARISON

The dimensions of the configurations proposed in Section 2 have been simulated and optimized. After fine-tuning and optimization, the final dimensions have been obtained and are listed in Table 1. Note that ΔH_u represents the difference between H_{ui} and H_{ui+1}.

Figure 12 shows photographs of the antenna. Fig. 13(a) presents the simulated and measured $|S_{11}|$. It is evident that the simulated and measured results are in good agreement, with a low cutoff frequency of 2.8 GHz obtained through testing. Moreover, the measured fractional bandwidth reaches 139%.

Figure 13(b) displays the simulated and measured gains, with the simulated gain reaching a maximum value of 10 dBi and the measured gain peaking at 9.3 dBi.

Figures 14(a)–(e) show the simulated and measured normalized E-plane/H-plane radiation patterns at different frequencies, demonstrating a high degree of consistency in terms of the main beam direction, 3 dB beamwidth, and sidelobe levels. The final manufactured antenna has physical dimensions of 140.96 mm $\times$ 85.39 mm $\times$ 0.508 mm ($7.18\lambda_g \times 4.35\lambda_g \times 0.03\lambda_g$), where λ_g represents the guided wavelength in the dielectric substrate at the center frequency of the operating band.

Compared to OAVA, the proposed antenna achieves a lower cutoff frequency and higher gain in the low frequency band, which is equivalent to achieving miniaturization. The performances of the proposed antenna and the other previous designs are listed in Table 2. It is evident that the proposed antenna exhibits the maximum value of low cutoff frequency reduction, thus validating the effectiveness of the proposed approach. However, in terms of other performance aspects of the antenna, designs in [1–3, 16] may have higher gains or lower low cutoff frequencies or wider FBWs. However, their covered frequency ranges are relative narrow. In comparison to [4, 5, 7, 8, 10, 12–14], the proposed antenna outperforms in terms of low cutoff frequency, FBW, and gain. Although the low cutoff frequencies in [6] and [11] are slightly lower than the proposed one, their gains are much lower. The antenna in [9, 24, 28] has an impressive gain. However, their low cutoff frequencies are high, and their FBWs are small. The antennas in [15] and [17] show that the gains are higher than this work. However, their profiles are relative high, which is unfavorable for planar integration. In

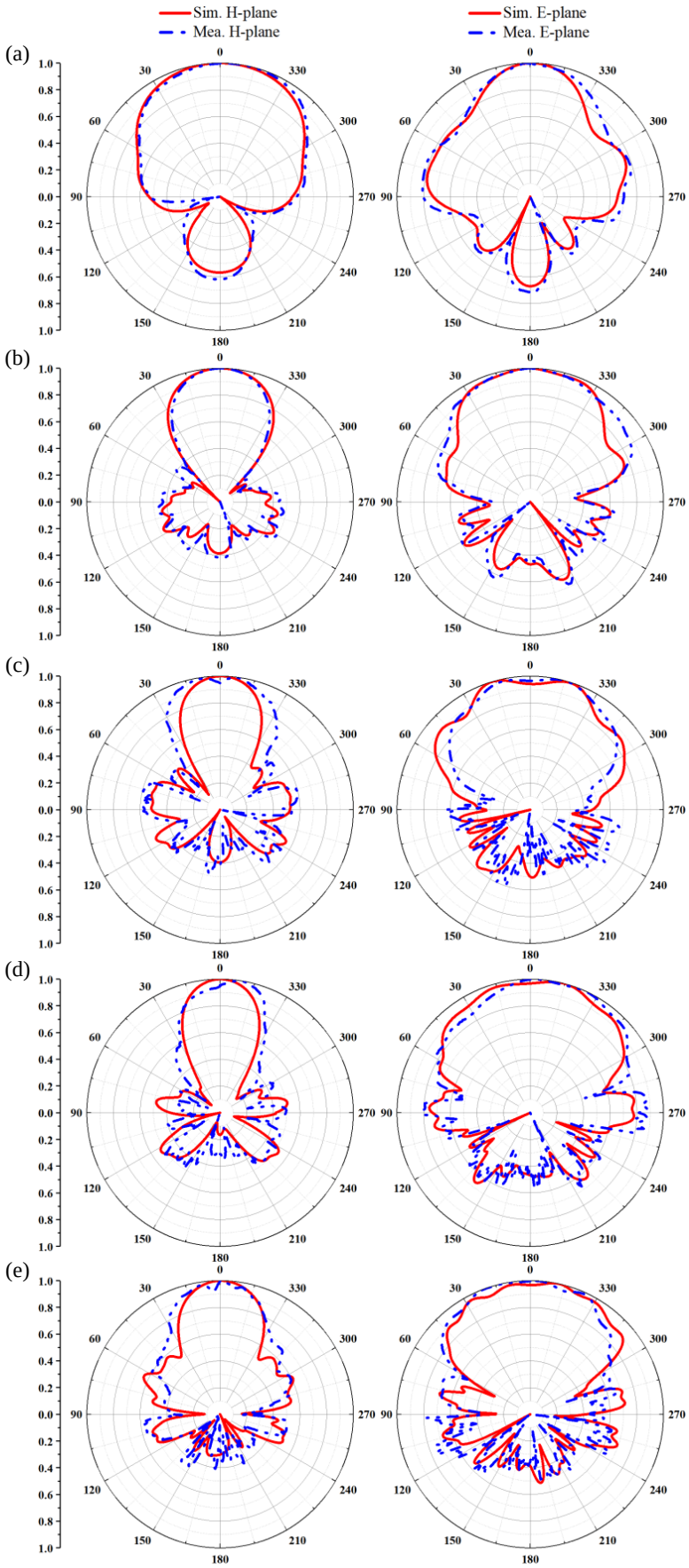

FIGURE 14. Simulated and measured normalized E-plane/H-plane radiation patterns of Antenna III at (a) 5 GHz, (b) 8 GHz, (c) 10.5 GHz, (d) 12 GHz, and (e) 15 GHz.

TABLE 2. Comparison of the proposed antenna.

Ref.	Bandwidth (GHz)	FBW (%)	Max Gain (dBi)	Volumn $(L(\lambda_g) \times W(\lambda_g) \times H(\lambda_g))$	Value of low cutoff frequency reduction (GHz)
[1]	24.6–28.5	14.69	11.32	$7.49 \times 3.6 \times 0.1$	0.1
[2]	0.3–2	147.83	11.5	$3.81 \times 2.86 \times 0.01$	0.06
[3]	1.5–3.3	75.00	8.41	$2.18 \times 2.18 \times 0.02$	0.03
[4]	6.0–12	66.67	8	$4.91 \times 1.96 \times 0.02$	/
[5]	3.1–10.6	109	5.5	$7.23 \times 2.89 \times 0.07$	/
[6]	1–20	181	7.8	$3.97 \times 4.48 \times 0.03$	/
[7]	4.5–8.5	62	7.9	$2.52 \times 2.04 \times 0.04$	0.12
[8]	3–15.1	90	7.7	$1.36 \times 1.6 \times 0.03$	/
[9]	6–18	100	12	$4.48 \times 3.42 \times 0.02$	/
[10]	2.9–13.55	129	6.9	$1.38 \times 0.93 \times 0.04$	0.2
[11]	0.8–12	175	6.32	$2.09 \times 1.06 \times 0.04$	/
[12]	3–8	91	9	$3.69 \times 3.22 \times 0.03$	0.198
[13]	4–12	100	6.3	$2.99 \times 1.99 \times 0.08$	0.3
[14]	2.5–8.5	109	7.5	$2.87 \times 1.86 \times 0.05$	1.1
[15]	4–16	120	15	$8.53 \times 3.11 \times 1.08$	/
[16]	24.75–27.5	19	9.3	$6.54 \times 3.39 \times 0.06$	1.08
[17]	3–10	108	11.8	$3.94 \times 3.94 \times 1$	0.31
[24]	3–14	129	13.8	$9.86 \times 3.36 \times 0.02$	/
[26]	2–40	181	10	/	/
[27]	2.4–14	141	10	$3.1 \times 2.48 \times 0.05$	0.9
[28]	3.1–11	112	10.2	$3.19 \times 3.19 \times 0.04$	/
[29]	5–20	120	9.9	$9.86 \times 4.37 \times 0.05$	/
This work	2.8–15.5	139	9.3	$7.18 \times 4.35 \times 0.03$	2.2

addition, the proposed antenna performs better than the work in [29] in terms of small volume, low cutoff frequency, and wide FBW. In all, the designed antenna exhibits the maximum value of low cutoff frequency reduction and offers various advantages in certain specifications compared with the works in literatures.

4. CONCLUSION

An antipodal Vivaldi antenna utilizing spoof surface plasmon polaritons (SSPPs) and corrugated edges with a lower cutoff frequency is designed and analyzed in this paper. Initially, a set of slots is etched on the outer edges of the traditional antipodal Vivaldi antenna, while simultaneously the SSPPs structure with a large propagation constant is etched on the inner side of the radiator, both intended to decrease the low cutoff frequency. To further enhance gain in high frequencies, a gradually disappearing corrugated structure etched on the inner side of the radiator is proposed to emit electromagnetic (EM) energy. The antenna described in this paper ultimately achieves a lower cutoff frequency, decreasing from 5 GHz to 2.8 GHz, without an increase in the physical dimensions of the antenna.

ACKNOWLEDGEMENT

This work is funded in part by the National Natural Science Foundation of China (62261022, 62361025), in part by the Project of Science and Technology Department of Jiangxi Province (20204BCJ23007), and in part by the Graduate Innovation Foundation of Jiangxi Province (No. YC 2022-S550).

REFERENCES

[1] Zhu, S., H. Liu, Z. Chen, and P. Wen, "A compact gain-enhanced Vivaldi antenna array with suppressed mutual coupling for 5G mmWave application," *IEEE Antennas and Wireless Propagation Letters*, Vol. 17, No. 5, 776–779, May 2018.

[2] Guo, J., J. Tong, Q. Zhao, J. Jiao, J. Huo, and C. Ma, "An ultrawide band antipodal Vivaldi antenna for airborne GPR application," *IEEE Geoscience and Remote Sensing Letters*, Vol. 16, No. 10, 1560–1564, Oct. 2019.

[3] De Oliveira, A. M., A. M. d. O. Neto, M. B. Perotoni, N. Nurhayati, H. Baudrand, A. d. Carvalho, and J. F. Justo, "A fern antipodal Vivaldi antenna for near-field microwave imaging medical applications," *IEEE Transactions on Antennas and Propagation*, Vol. 69, No. 12, 8816–8829, Dec. 2021.

[4] Stern, F., W. Taute, R. Knöchel, and M. Höft, "Dual antipodal Vivaldi antenna based moisture sensor for industrial process con-

trol," *IEEE Sensors Journal*, Vol. 23, No. 19, 22 430–22 439, Oct. 2023.

[5] Hood, A. Z., T. Karacolak, and E. Topsakal, "A small antipodal Vivaldi antenna for ultrawide-band applications," *IEEE Antennas and Wireless Propagation Letters*, Vol. 7, 656–660, Mar. 2008.

[6] Deng, C. and Y.-J. Xie, "Design of resistive loading Vivaldi antenna," *IEEE Antennas and Wireless Propagation Letters*, Vol. 8, 240–243, Jan. 2009.

[7] Abbak, M., M. Çayören, and I. Akduman, "Microwave breast phantom measurements with a cavity-backed Vivaldi antenna," *IET Microwaves, Antennas & Propagation*, Vol. 8, No. 13, 1127–1133, Oct. 2014.

[8] Wu, J., Z. Zhao, Z. Nie, and Q.-H. Liu, "A printed UWB Vivaldi antenna using stepped connection structure between slotline and tapered patches," *IEEE Antennas and Wireless Propagation Letters*, Vol. 13, 698–701, Apr. 2014.

[9] Sang, L., S. Wu, G. Liu, J. Wang, and W. Huang, "High-gain UWB Vivaldi antenna loaded with reconfigurable 3-D phase adjusting unit lens," *IEEE Antennas and Wireless Propagation Letters*, Vol. 19, No. 2, 322–326, Feb. 2020.

[10] Saleh, S., W. Ismail, I. S. Z. Abidin, M. H. Jamaluddin, M. H. Bataineh, and A. S. Al-Zoubi, "Novel compact UWB Vivaldi nonuniform slot antenna with enhanced bandwidth," *IEEE Transactions on Antennas and Propagation*, Vol. 70, No. 8, 6592–6603, Aug. 2022.

[11] Schneider, J., M. Mrnka, J. Gamec, M. Gamcova, and Z. Raida, "Vivaldi antenna for RF energy harvesting," *Radioengineering*, Vol. 25, No. 4, 666–671, Sep. 2016.

[12] Wang, J., J. Liu, Y. Fan, and Y. Bai, "A novel Vivaldi antenna for UWB detection," *Microwave and Optical Technology Letters*, Vol. 65, No. 3, 826–843, Mar. 2023.

[13] Rajesh, N., K. Malathi, S. Raju, V. A. Kumar, S. D. R. Prasath, and M. G. N. Alsath, "Design of Vivaldi antenna with wideband radar cross section reduction," *IEEE Transactions on Antennas and Propagation*, Vol. 65, No. 4, 2102–2105, Apr. 2017.

[14] Ren, J., H. Fan, Q. Tang, Z. Yu, Y. Xiao, and X. Zhou, "An ultra-wideband Vivaldi antenna system for long-distance electromagnetic detection," *Applied Sciences*, Vol. 12, No. 1, 528–542, Jan. 2022.

[15] Ding, M., X. Wang, Y. S. Wang, Z. Hu, G. Liu, Z. Liu, and B. Wang, "A high gain Vivaldi antenna with multiple near-field dielectric lenses and grooved edges," *International Journal of RF and Microwave Computer-Aided Engineering*, Vol. 2023, 11–22, May 2023.

[16] Liu, H., W. Yang, A. Zhang, S. Zhu, Z. Wang, and T. Huang, "A miniaturized gain-enhanced antipodal Vivaldi antenna and its array for 5G communication applications," *IEEE Access*, Vol. 6, 76 282–76 288, Nov. 2018.

[17] Wang, J., J. Liu, K. Hou, and Y. Li, "A novel antipodal Vivaldi antenna for ultra-wideband far-field detection," *AEU — International Journal of Electronics and Communications*, Vol. 164, 154626, 2023.

[18] Yang, L., F. Xu, T. Jiang, J. Qiang, S. Liu, and J. Zhan, "A wideband high-gain endfire antenna based on spoof surface plasmon polaritons," *IEEE Antennas and Wireless Propagation Letters*, Vol. 19, No. 12, 2522–2525, Dec. 2020.

[19] Pitarke, J. M., V. M. Silkin, E. V. Chulkov, and P. M. Echenique, "Theory of surface plasmons and surface-plasmon polaritons," *Reports on Progress in Physics*, Vol. 70, No. 1, 1–87, May 2007.

[20] Yang, Y., Z. Li, S. Wang, X. Chen, J. Wang, and Y. J. Guo, "Miniaturized high-order-mode dipole antennas based on spoof surface plasmon polaritons," *IEEE Antennas and Wireless Propagation Letters*, Vol. 17, No. 12, 2409–2413, Dec. 2018.

[21] Qu, B., S. Yan, A. Zhang, Y. Pang, and Z. Xu, "Miniaturization of monopole antenna based on spoof surface plasmon polaritons," *IEEE Antennas and Wireless Propagation Letters*, Vol. 20, No. 8, 1562–1566, Aug. 2021.

[22] Cheng, Z. W., J. Deng, M. Wang, J. R. Chen, S. Wang, S. Luan, X. Liu, F. Gao, H. F. Ma, and T. J. Cui, "A compact axial-mode helical antenna based on spoof surface plasmon polaritons," *IEEE Transactions on Antennas and Propagation*, Vol. 71, No. 7, 5582–5590, Jul. 2023.

[23] Fu, Q., H. Ni, G. Q. Luo, L. Zhu, and L. Liu, "A high aperture efficiency endfire antenna based on spoof surface plasmon polaritons," *IEEE Transactions on Antennas and Propagation*, Vol. 71, No. 1, 50–57, Jan. 2023.

[24] Liao, Z., Y. Z. Che, G. Q. Luo, Z. H. Zhang, Y. H. Qian, and B. G. Cai, "Enhanced radiation characteristics for Vivaldi antenna using spoof surface plasmon polaritons," *IEEE Transactions on Plasma Science*, Vol. 49, No. 9, 2730–2736, Sep. 2021.

[25] Liu, L., M. Chen, and X. Yin, "Single-layer high gain endfire antenna based on spoof surface plasmon polaritons," *IEEE Access*, Vol. 8, 64 139–64 144, Mar. 2020.

[26] Gibson, P. J., "The Vivaldi aerial," in *1979 9th European Microwave Conference*, 101–105, Brighton, UK, 1979.

[27] Fei, P., Y.-C. Jiao, W. Hu, and F.-S. Zhang, "A miniaturized antipodal Vivaldi antenna with improved radiation characteristics," *IEEE Antennas and Wireless Propagation Letters*, Vol. 10, 127–130, 2011.

[28] Abbosh, A. M., H. K. Kan, and M. E. Bialkowski, "Design of compact directive ultra wideband antipodal antenna," *Microwave and Optical Technology Letters*, Vol. 48, No. 12, 2448–2450, Dec. 2006.

[29] Yin, J. Y., H. C. Zhang, Y. Fan, and T. J. Cui, "Direct radiations of surface plasmon polariton waves by gradient groove depth and flaring metal structure," *IEEE Antennas and Wireless Propagation Letters*, Vol. 15, 865–868, 2015.